Original article

*Resolution and Discovery*
*DOI: 10.1556/2051.2016.00035*

# MICROSTRUCTURE OF SILICON NANORODS FOR NOVEL SOLAR CELLS

**G. Z. Radnóczi[1]*, Th. Stelzner[2], V. A. Sivakov[2], J. Stoimenos[3], S. H. Christiansen[2,4], B. Pécz[1]**

[1]Institute for Technical Physics and Materials Science, Centre for Energy Research, Hungarian Academy of Sciences, H-1525 Budapest, P.O. Box 49, Hungary
[2]Leibniz-Institut für Photonische Technologien, Albert Einstein Str. 9, D-07745, Jena, Germany
[3]Department of Physics, Aristotle University of Thessaloniki, GR-54124, Thessaloniki, Greece
[4]MaxPlanck Institut für die Physik des Lichts, Günther Scharowsky Str. 1, 91058 Erlangen, Germany

Received: 30 May, 2016; Accepted: 07 July, 2016

Silicon nanorods were produced by the vapor–liquid–solid process and by wet chemical etching as possible candidates for solar cells. The nanostructures of Si nanorods formed by the two different processes are investigated and compared by transmission electron microscopy. The first type of nanorods was formed from bulk Si by wet-chemical top-down etching using Ag particles as catalyst. They exhibit a perfect crystalline structure but a wide distribution of diameter. The cross section of these rods is irregular, no faceting is observed, and the shape of the cross section depends on the random arrangement of the Ag particles. The etched rods are mostly parallel to the substrate normal as it is expected. The second type of nanorods was grown on Si substrate by the bottom-up vapor–liquid–solid method using gold as a catalyst and silane as silicon source. These nanorods exhibit a single crystalline structure with twin boundaries and some kinks. The cross section of these rods is almost circular, but faceting is often observed.

**Keywords:** silicon, nanorod, solar cell, transmission electron microscopy, VLS growth, catalyst

## Introduction

Silicon-based solar cells are favored, thanks to the non-toxicity of the material and also due to the well-developed silicon technology. During the last decade, silicon nanorods (SiNRs) gained a great interest in several applications, for example, sensors [1, 2], and also as solar cell materials [3–7]. Such good quality, mostly single-crystalline and defect-free semiconductor nanostructures can be used as building blocks of novel semiconductor devices. Near-zero reflection over a broad range of incident angles is obtained by forming a density-graded layer with features smaller than the wavelength of light [8], which eliminates the need for conventional vacuum-deposited antireflection coatings.

The required material for growing such a forest is also much less than the volume of bulk structures since NRs can be grown on any cheap substrate that is sufficiently stable at growth temperatures.

The most favored way to grow SiNRs is the vapor–liquid–solid (VLS) growth [9] in which Si nanorods are grown under a gold droplet supersaturated by silicon from a gas phase. Using gold as a catalyst in the VLS process SiNRs usually leads to <111> or <211> growth direction depending on growth conditions. VLS grown silicon nanorods are compared to those ones, which are etched from a silicon wafer by wet chemical etching using silver nanoparticles, as a catalyst [10–12]. The crystallography, morphology, and microstructure of silicon nanorods are studied by transmission electron microscopy (TEM) and discussed in detail in the present paper.

## Materials and methods

Low boron doped p-Si(111) wafers were used for the wet-chemical etching technique. Wafers were cleaned in acetone and ethanol for 2 + 2 min, and then, the native oxide was removed by a short treatment in 40% hydrogen fluoride (HF) followed by a 1-min rinse in 2% HF. Finally, the wafers were cleaned from the remaining HF by deionized water and blow dried. This cleaning process results in a hydrogen terminated surface which may prevent oxidation of the silicon surface for a few minutes under atmospheric conditions. This allowed silver deposition on practically oxide free Si surfaces. Silver nanoparticles were deposited on the substrate by immersion into an aqueous solution of 0.02 M silver nitrate and 5 M HF. Then, the wafer was immersed in a second etching solution containing a mixture of 5 M HF and 30% $H_2O_2$ in a volume ratio of 10:1. In this step, the Ag particles etch channels into the silicon and practically sink into the substrate. The process is driven by the fact that silver nanoparticles catalytically decompose hydrogen peroxide

* Corresponding author: G. Z. Radnóczi; E-mail: gy.radn@mfa.kfki.hu

($H_2O_2$) [13]. After the etching steps, SiNR surfaces were rinsed in deionized water and dried. To remove the silver particles from the structure, the wafer was immersed in 65% nitric acid for a couple of minutes.

Silicon nanowires were also prepared by the vapor–liquid–solid (VLS) method using chemical vapor deposition (CVD) from silane ($SiH_4$) under two different conditions. In the first, a low doped n-Si(111) surface was treated in diluted HF and then annealed in a molecular beam epitaxy (MBE) chamber at 830 °C and a pressure of about $10^{-9}$ mbar for 20 min to remove the native oxide. Subsequently, a 0.5-nm-thick Au film was deposited on the substrate by MBE at a temperature of ~510 °C. Then, the specimen was transferred into the CVD chamber and annealed at 580 °C in high vacuum ($1 \times 10^{-7}$ mbar) for 10 min. The temperature was then reduced to ~510 °C, and the process gas (5 sccm Ar; 4 sccm $SiH_4$; total pressure, 0.5 mbar; low silane partial pressure, ~0.27 mbar) was introduced for the nanowire growth for 20 min. In the second experiment, 150 nm Au colloids (British Biocell Int.) were directly deposited onto low doped n-Si(111) substrate using a self-assembly technique and silane chemistry [14]. The samples were transferred into the CVD chamber and annealed at 580 °C in a high vacuum ($1 \times 10^{-7}$ mbar) for 10 min. The temperature was reduced to ~510 °C, then the process gas was introduced (10 sccm Ar; 5 sccm $SiH_4$; high silane partial pressure, ~0.66 mbar; total pressure, 2 mbar), and NWs were grown for 20 min.

Microscopy was carried out on two transmission electron microscopes (TEM), a Philips CM20 analytical microscope operating at 200 kV, and used for diffraction contrast imaging and a JEOL 3010 high-resolution microscope equipped with a Gatan Imaging Filter operating at 300 kV. Specimens for TEM investigations were prepared in two ways. In the first process, nanorods were harvested from the substrate in an ultrasonic bath of deionized water, and then, a droplet of the suspension was placed on a lacey carbon grid. When preparing a TEM specimen this way, one should keep in mind that the process may be selective; there may be structures grown onto the substrate that will not detach from it or some structures might be lost (e.g., broken into too small pieces) during the process. In the second process, the structure is filled up by a low viscosity embedding glue (M-Bond 610) by covering the whole structure with a thin (typically 20–50 μm) layer of the glue. Then, conventional $Ar^+$ ion milling was carried out to obtain various thin sections of the embedded structures. Ion energies were typically in the range of 6–10 keV; lower energies were applied before reaching perforation of the specimen to avoid excessive heat load on the nanorods. To remove amorphous artifacts, low energy ion milling was carried out on most samples in the range of 500–2000 eV. On plan-view TEM specimens (sections parallel to the substrate), the ion milling procedure described in Refs. 15 and 16 was followed to obtain thin sections lying deeper than the embedding glue surface.

## Results and discussion

*Wet chemically etched SiNRs*

Typical cross-sectional TEM view of wet chemically etched silicon nanorods are shown in *Figure 1*. The micrograph was taken on an ion-milled cross section of the structure as described in the experimental section. The shown thin section is approximately perpendicular to the substrate surface, and the imaging electron beam is parallel with the substrate surface; hence, we see a forest of SiNRs perpendicular to the substrate surface, with straight vertical boundaries. On the dark field micrograph (*Figure 1b*), it is evident that there is no boundary at the substrate since the structure was natively the same piece of single crystalline material.

All the etched channels have a depth of 2.7 ± 0.3 μm. The very short NR denoted by an arrow in *Figure 1* is most probably a part of a full length NR which has lost its top section during preparation. The diameter of the NRs is rather diverse, ranging from 330 to 43 nm, depending on the size and arrangement of the silver grains. An NR transferred to lacey carbon grid is shown at high magnification in *Figure 2*.

The NR exhibits a straight surface with exceptionally occurring rougher regions denoted by an arrow in *Figure 2*. Contours along the axis are usually seen, which are attributed to thickness variations due to irregular cross sections. As originally, these pieces of Si belonged to one single crystal, no twins or other defects were observed in these NRs. To image the cross section of the NRs, a thin section of the structure was prepared parallel to the substrate surface. The image showing several chemically etched nanorods is shown in *Figure 3*. These have irregular cross sections and a wide range of diameters (from 50 to 1000 nm). This is a consequence of the more or less random arrangement of the Ag catalyst particles which promote the etching process. This way, the cross section of the remaining material will have an irregular concave shape, which necessitates further process steps to reach cross sections more suitable for solar cell applications. The structure obtained here has a relatively large surface area, that may be advantageous in other applications, e.g., sensors.

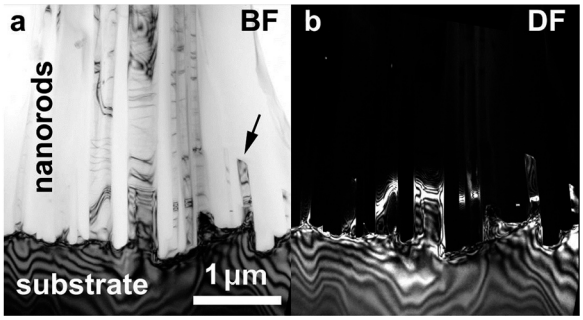


**Fig. 1.** Wet chemically etched SiNRs imaged on a cross-sectional TEM specimen in bright field (BF) and in dark field image (DF). These SiNRs are single crystalline and defect free

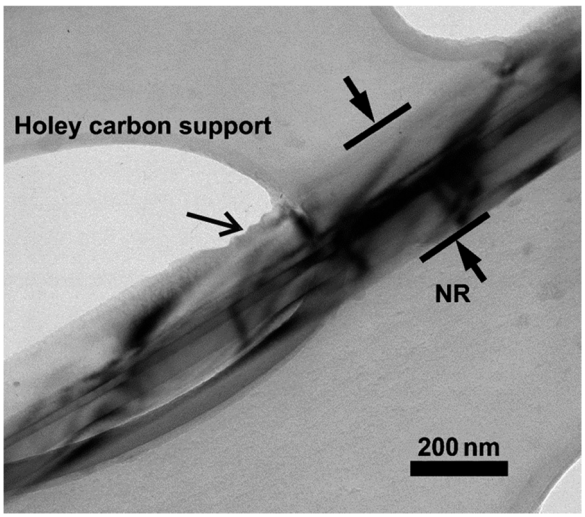


**Fig. 2.** TEM micrograph of wet chemically etched SiNR on lacy carbon grid. The NR exhibits a smooth surface; however, as exception, rougher regions appear denoted by an arrow. Contours along the NRs are visible due to irregular cross section

*SiNRs grown by the VLS method*

The VLS grown structures contain NRs that are grown in random directions with respect to the substrate as shown in *Figure 4*. On the ion-milled thin sections shown in *Figure 4*, many different sections of NRs are seen depending on the NRs angle with respect to the thin section's plane which is approximately perpendicular to the substrate surface. At low silane partial pressure (*Figure 4a*), SiNRs were grown on a native oxide free Si wafer having their axis along the <111> direction. In contrast, the NRs grown at higher silane partial pressure grow along the <211> direction and planar defects are seen along the axis of one NR shown in *Figure 4b*. From this image, it is clearly seen that proper side view of the structure can only result from a different preparation method, ensuring that the NRs lie in a plane perpendicular to the imaging electron beam. To achieve this, some of the NRs were transferred to amorphous carbon foil. *Figure 5* shows a collection of results obtained on NRs grown at low silane partial pressure.

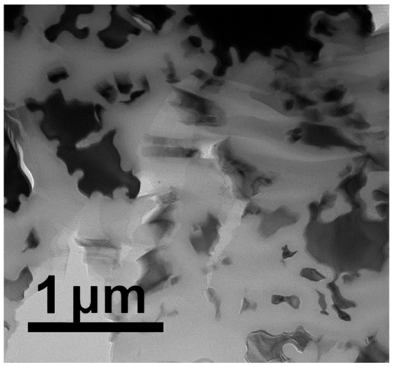


**Fig. 3.** Bright field TEM micrograph of the cross sections of SiNRs. The dark irregular shapes are images of crystalline silicon slices, and the glue is imaged as a light gray matrix

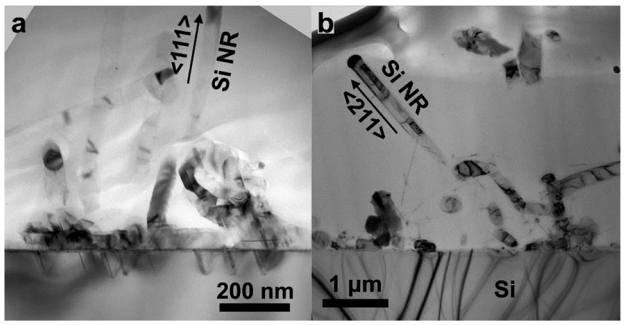


**Fig. 4.** Cross-sectional micrograph of VLS grown NRs with preferred <111> growth direction along the axis (a) and VLS SiNRs grown along the <211> direction (b). The presence of twins is clearly visible in the NRs grown along the <211> direction

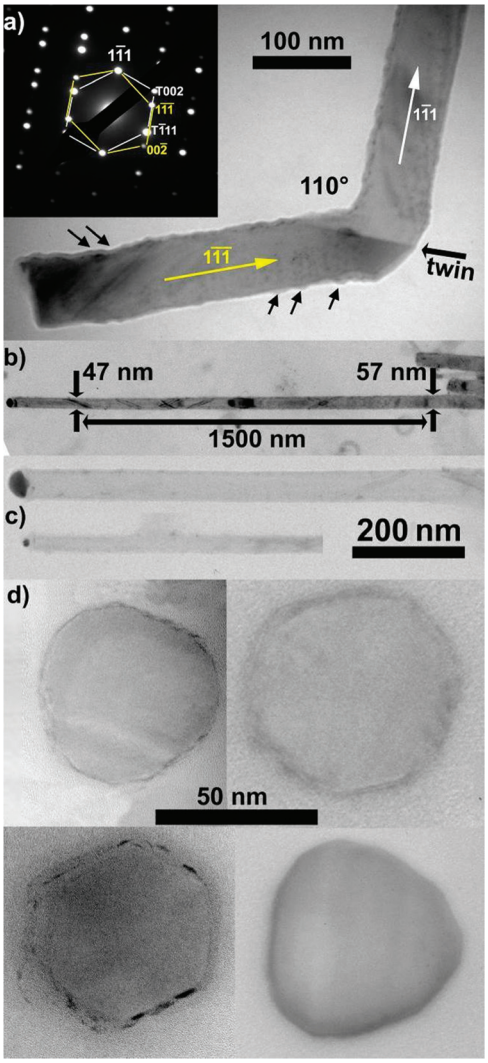


**Fig. 5.** TEM micrographs of SiNRs grown at low silane partial pressure along the <111> direction. In (a), a typical kink is shown with an angle of approximately 110°. There is also a twin boundary near the kink as revealed by the selected area electron diffraction. The corresponding diffraction pattern is shown in the inset; the twin spots are denoted by the letter T. (b) SiNRs tend to decrease in diameter towards the tip with the gold catalyst particle. (c) NRs with different diameter determined by the size of the gold catalyst particle. (d) Cross sections of SiNRs exhibiting side wall facets

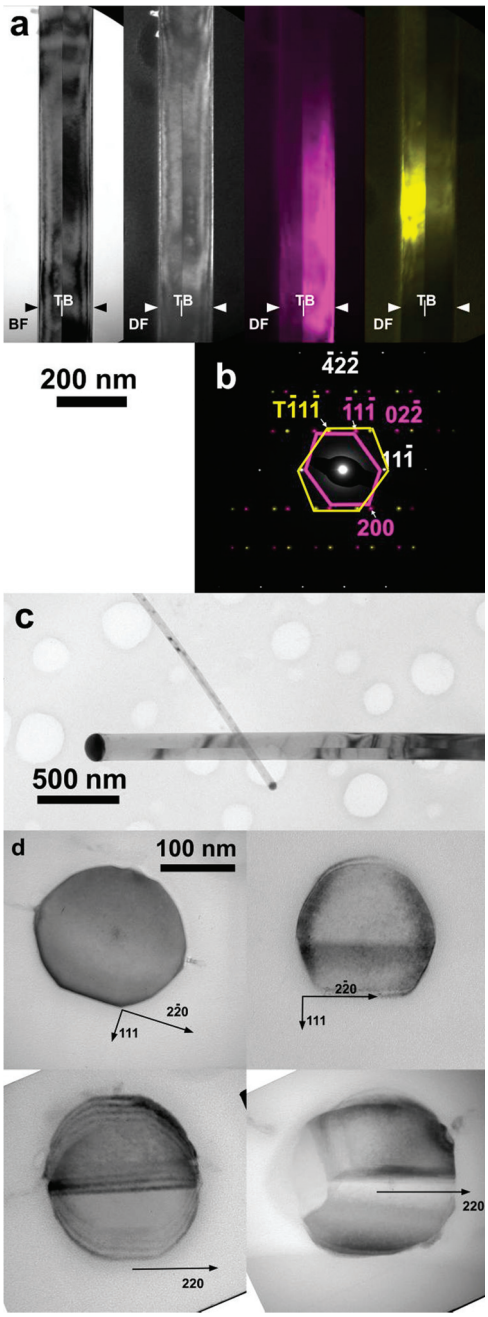


**Fig. 6.** TEM micrographs of NRs grown at high silane partial pressure, along the <211> direction. (a) A usual twin boundary is imaged in bright field and dark field. The first dark field image (gray) is taken with the common (11-1) reflection (white index), and the yellow and purple colored ones were taken selecting reflections only active in the respective member of the twins. The purple and yellow color coding shows the corresponding scattering volumes and reflections in the SAED pattern. (b) A <111> twin boundary is revealed being parallel with the NR axis. (c) Two NRs with different size Au catalyst particles and diameters matching the catalyst. Also, twin boundaries are visible in the NRs. (d) Cross sections of NRs exhibiting <111> facets and twin boundaries

The formation of (111)-type twins and the change of the growth direction are shown in *Figure 5a*. These kinks form while the growth direction changes from one <111>-type direction to another equivalent one (there is an angle of 109.5° between different <111>-type directions.) The angle of the kink presented in *Figure 5a* is 110° being very close to the theoretical value mentioned above. The inset in *Figure 5a* is a selected area diffraction pattern showing two different <110> zones with a common {111} mirror plane being also the twin boundary plane. The two sets of reflections corresponding to the respective member of the twins are connected with white and yellow lines. The roughness of the sidewalls, shown by arrows, is also revealed; surface irregularities extend to a range of about 5–10 nm. The surface roughness is attributed to small changes of the diameter of the Au droplet during the growth [17].

The diameter of Si NRs is depending on the Au catalyst particle's diameter as seen in *Figure 5c*. A slight change in the diameter of the NRs along the growth direction is also observed (*Figure 5b*). The diameter is decreasing by about its fifth (10 nm) over a distance of 1500 nm. This may be attributed to two reasons: (1) the catalyst particle is decreasing in size during the growth process, so-called Ostwald ripening [18] takes place, or gold is evaporating or trapped in the growing Si phase; (2) the sidewalls are epitaxially growing at a slow rate during the process. The latter explanation is less probable since we do not see any growth on the substrate surface, although there should be considerable deposition of Si there as well if there is one on the side walls. Assuming the catalyst particle is decreasing during the process implies a limit for the length of the rods set by the point where the catalyst particle is consumed. It is difficult to determine the reason for the shrinkage of the Au particle. There are Au atoms in a solid solution in the NR, and their undesirable effect on electrical properties are also known [19, 20]; however, this means a low concentration (in the order of the dopant concentration levels) that cannot account for a visible shrinkage. Evaporation of the catalyst material will also occur in a slow rate determined by the low equilibrium vapor pressure of Au (~$10^{-8}$ mbar at 510 °C) at the growth temperature. Taking the large surface to volume ratio of the catalyst particles into account, it seems reasonable to suggest that evaporation of Au is one possible reason for the shrinking of the catalyst particles.

Other studies [21] also mention surface diffusion of Au atoms on the sidewalls, leading to Ostwald ripening. Although we do not observe NRs increasing in diameter during growth (which would prove Ostwald ripening), it is reasonable to assume that sidewalls accommodate a small amount of gold that could also contribute to the shrinkage. Nevertheless, recent studies on gold contamination in SiNWs, based on grazing-incidence X-ray diffraction [22], revealed that a significant amount of gold is present on the sidewalls of the NRs even after a wet-chemical etching process meant to remove the gold contamination. The cross section of the NRs was also studied on ion-milled plan view sections of the structure embedded in glue. The slices of NRs are shown in *Figure 5d*. All of them have low-energy silicon facets with a morphology close to six- or three-fold symmetry. High-resolution images showed that {220} lattice fringes are present

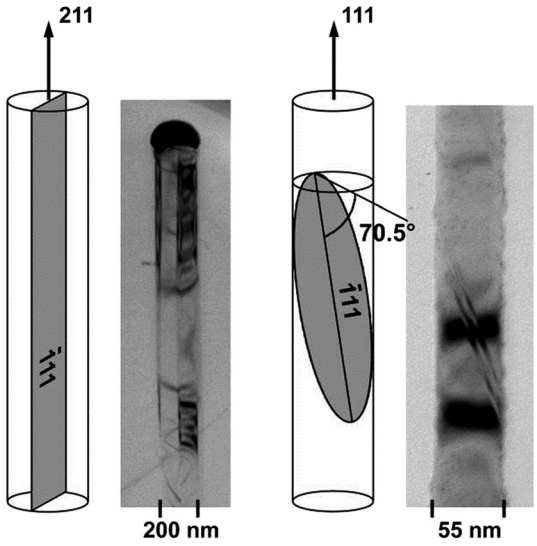


**Fig. 7.** Alignment of the {111} plane twin boundaries in NRs grown in <211> and <111> directions and examples on observed twin boundaries. If the axis is parallel with the <211> direction, the twin boundary will also be parallel with the axis extending over the whole NR. In NRs grown along the <111> direction, the twin boundaries are tilted with respect to the axis

perpendicular and 30° off the facet planes. From this, we conclude that the side facets are of {112} type where the cross section is hexagonal.

Si NRs grown at high silane partial pressure on (111) Si wafers with the native oxide present exhibit strong [211] preferred orientation as shown in *Figure 6*.

Twinning is also observed here, but the different orientation of the growth axis constrains the (111) plane twin boundaries to be parallel with the axis. Such a twin boundary is presented in *Figure 6a*. The first image is a bright field micrograph with the electron beam parallel to [022] direction, followed by three dark field images. Dark field images were recorded with diffracted beams as follows: 1. common (11-1) — in this case, the twin boundary (TB) is almost invisible; 2. purple colored (02-2) — only the right side of the twin SiNR is visible; 3. yellow colored — twin reflection (T-11-1) reveals the left side of the twin.

Due to the geometry of the twin boundary, the rods are cut to halves by a boundary extending over the whole length (*Figure 6c*). Cross sections of these NRs were also prepared to examine the shape of sidewalls. These are different from those grown at low silane partial pressure having more round sections and sidewall facets of only <111> type, that are smoother, and facets are parallel with the twin boundary.

A comparison of the twin geometry in the two types of VLS grown NRs is presented in *Figure 7*. In <111> NRs, twins must be at an angle (or perpendicular) to the axis, and hence, they can only extend over a section of the rod in contrast to the usual case for <211> rods. Obviously, the twin formation takes place at an early stage of the growth and the position of the boundary within the NR is maintained for very long sections, indicating that the growth direction is also maintained accurately during growth.

## Conclusions

Silicon nanorods for solar cell applications were produced successfully in two different ways, investigated in detail, and compared in view of their structural properties. Top-down NRs exhibit a perfect crystalline quality and alignment inherited from the original single crystalline wafer; however, the shape of their cross section is irregular (that can be possibly controlled by silver pattering). In comparison, bottom-up VLS grown nanorods have a uniform morphology, while there is no uniform alignment of the rods when epitaxial growth is disturbed. During the VLS growth, defects are formed in the Si wire. Two types of defects were observed: kinks and twin boundaries.

Axial p–n junctions can be prepared from both types of the grown Si NRs. Radial p–n junctions could be formed on the VLS grown nanowires while that could be more difficult on the etched ones due to the irregular concave side surface and wide distribution of diameter. Once the NR morphology can be controlled in a reliable and simple way, the etched structure becomes a promising candidate for solar cell fabrication. The VLS grown NRs exhibit an advantageous morphology; however, their alignment is not uniform which may set back their application. Furthermore, gold catalyst can influence the electrical properties of the wires via deep levels in Si, and therefore, further experiments are in progress with different catalyst material.

## Acknowledgment

The authors acknowledge the support of the European Commission in the ROD_SOL FP7 project. B. Pécz thanks the financial support of the OTKA project (Hungary) No. K 108869.

## References

1. Duan X, Huang Y, Cui Y, Wang J, Lieber CM: Indium phosphide nanowires as building blocks for nanoscale electronic and optoelectronic devices. Nature 409, 66–69 (2001)
2. Gudiksen MS, Wang J, Lieber CM: Synthetic control of the diameter and length of single crystal semiconductor nanowires. J Phys Chem B 105, 4062–4064 (2001)
3. Sivakov V, Andrä G, Gawlik A, Berger A, Plentz J, Falk F, Christiansen SH: Silicon nanowire-based solar cells on glass: synthesis, optical properties, and cell parameters. Nano Lett 9, 1549–1554 (2009)
4. Tsakalakos L, Balch J, Fronheiser J, Korevaar A, Sulima O, Rand J: Silicon nanowire solar cells. Appl Phys Lett 91, 233117 (2007)
5. Kayes BM, Lewis NS, Atwater HA: Comparison of the device physics principles of planar and radial p–n junction nanorod solar cells. J Appl Phys 97, 114302 (2005)
6. Sivakov V, Voigt F, Hoffmann B, Gerliz V, Christiansen S: Wet – chemically etched silicon nanowire architectures: formation and properties. In Hashim A (Ed.) *Nanowires — Fundamental Research*. Intech, Rijeka 2011, pp 45–80

7. Oh J, Yuan H-C, Branz HM: An 18.2%-efficient black-silicon solar cell achieved through control of carrier recombination in nanostructures. Nat Nanotechnol 7, 743–748 (2012)
8. Branz HM, Yost VE, Ward S, Jones KM, To B, Stradins P: Nanostructured black silicon and the optical reflectance of graded-density surfaces. Appl Phys Lett 94, 231121 (2009)
9. Wagner RS, Ellis WC: Vapor–liquid–solid mechanism of single crystal growth. Appl Phys Lett 4, 89 (1964)
10. Huang Z, Zhang X, Reiche M, Liu L, Lee W, Shimizu T, Senz S, Gösele U: Extended arrays of vertically aligned sub-10 nm diameter [100] Si nanowires by metal-assisted chemical etching. Nano Lett 8, 3046 (2008)
11. Peng KQ, Wu Y, Fang H, Zhong XY, Xu Y, Zhu J: Uniform, axial-orientation alignment of one-dimensional single-crystal silicon nanostructure arrays. Angew Chem Int Ed 44, 18, 2737–2742 (2005)
12. Fang H, Wu Y, Zhao J, Zhu J: Silver catalysis in the fabrication of silicon nanowire arrays. Nanotechnology 17, 378–3774 (2006)
13. Sivakov VA, Bronstrup G, Pecz B, Berger A, Radnoczi GZ, Krause M, Christiansen SH: Realization of vertical and zigzag single crystalline silicon nanowire architectures. J Phys Chem. C 114, 3798–3803 (2010)
14. Knauer A, Thete A, Li S, Romanus H, Csáki A, Fritzsche W, Köhler J: Au/Ag/Au double shell nanoparticles with narrow size distribution obtained by continuous micro segmented flow synthesis. Chem Eng J 166, 1164–1169 (2011)
15. Sáfrán G, Grenet T: Novel method for the plan-view TEM preparation of thin samples on brittle substrates by mechanical and ion beam thinning. Microsc Res Tech 56, 308–314 (2002)
16. Radnóczi GZ, Pécz B: Transmission electron microscope specimen preparation for exploring the buried interfaces in plan view. J Microsc 224, 328–331 (2006)
17. Shi J, Wang X: Functional semiconductor nanowires via vapor deposition. J Vac Sci Technol B 29, 060801 (2011)
18. Gösele U: Nanotechnology: how clean is too clean? Nature 440, 34 (2006)
19. Allen JE, Hemesath ER, Perea DE, Lensch-Falk JL, Li ZY, Yin F, Gass MH, Wang P, Bleloch AL, Palmer RE, Lauhon LJ: High-resolution detection of Au catalyst atoms in Si nanowires. Nat Nanotechnol 3, 168–173 (2008)
20. Putnam MC, Filler MA, Kayes BM, Kelzenberg MD, Guan Y, Lewis NS, Eiler JM, Atwater HA: Secondary ion mass spectrometry of vapor–liquid–solid grown, Au-catalyzed, Si wires. Nano Lett 8, 3109 (2008)
21. Hannon JB, Kodambaka S, Ross FM, Tromp RM: The influence of the surface migration of gold on the growth of silicon nanowires. Nature 440, 69–71 (2006)
22. Dupre L, Buttard D, Leclere C, Renevier H, Gentile P: Gold contamination in VLS-grown Si nanowires: multiwavelength anomalous diffraction investigations. Chem Mater 24, 4511 (2012)